Article

An Artificial Metalloenzyme Based on a Copper Heteroscorpionate Enables sp³ C−H Functionalization via Intramolecular Carbene Insertion

Corentin Rumo, Alina Stein, Juliane Klehr, Ryo Tachibana, Alessandro Prescimone, Daniel Häussinger, and Thomas R. Ward*

ACCESS | Metrics & More | Article Recommendations | SI Supporting Information

ABSTRACT: The selective functionalization of sp³ C−H bonds is a versatile tool for the diversification of organic compounds. Combining attractive features of homogeneous and enzymatic catalysts, artificial metalloenzymes offer an ideal means to selectively modify these inert motifs. Herein, we report on a copper(I) heteroscorpionate complex embedded within streptavidin that catalyzes the intramolecular insertion of a carbene into sp³ C−H bonds. Target residues for genetic optimization of the artificial metalloenzyme were identified by quantum mechanics/ molecular mechanics simulations. Double-saturation mutagenesis yielded detailed insight on the contribution of individual amino acids on the activity and the selectivity of the artificial metalloenzyme. Mutagenesis at a third position afforded a set of artificial metalloenzymes that catalyze the enantio- and regioselective formation of β- and γ-lactams with high turnovers and promising enantioselectivities.
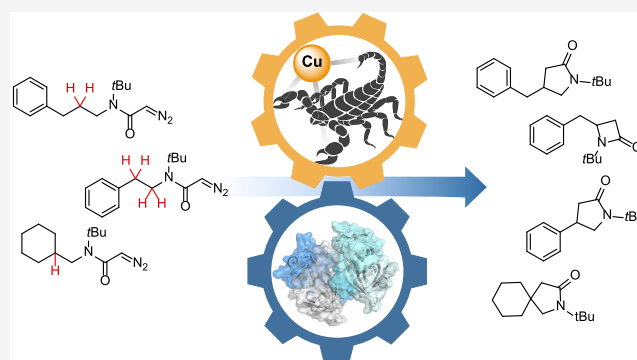
INTRODUCTION

The selective functionalization of inert C−H bonds currently lies at the forefront of modern synthetic chemistry. It alleviates the laborious interconversion of functional groups, minimizes the number of synthetic steps, and enables capitalizing on previously inaccessible bond formation strategies.[1−3] This reduces the environmental footprint of lengthy chemical processes.

Thus far, the field of homogeneous C−H functionalization has been mostly dominated by precious-metal catalysts used in combination with directing groups and is often performed at elevated temperatures.[4] One of the recurring challenges faced with such methodologies is the reductive elimination of the stable M−C bond.[5] An attractive approach to circumvent this limitation is the insertion of a reactive M−X species into the C−H bond of a substrate that does not interact with the metal (Scheme S1).[6−9] Largely developed by Pérez and co-workers, complexes bearing a tris(pyrazolyl)borate (Tp) ligand have been shown to enable the functionalization of simple alkanes with carbene, nitrene, and oxo intermediates.[9−11] The pyrazole motif offers the possibility to readily fine-tune both steric and electronic properties of the TpM-catalyst to achieve the desired reactivity. Remarkably, perfluorinated azolylborate complexes of silver and copper catalyze the functionalization of methane in supercritical CO_2 with ethyl diazoacetate.[12,13] However, this system occasionally yielded complex mixtures of
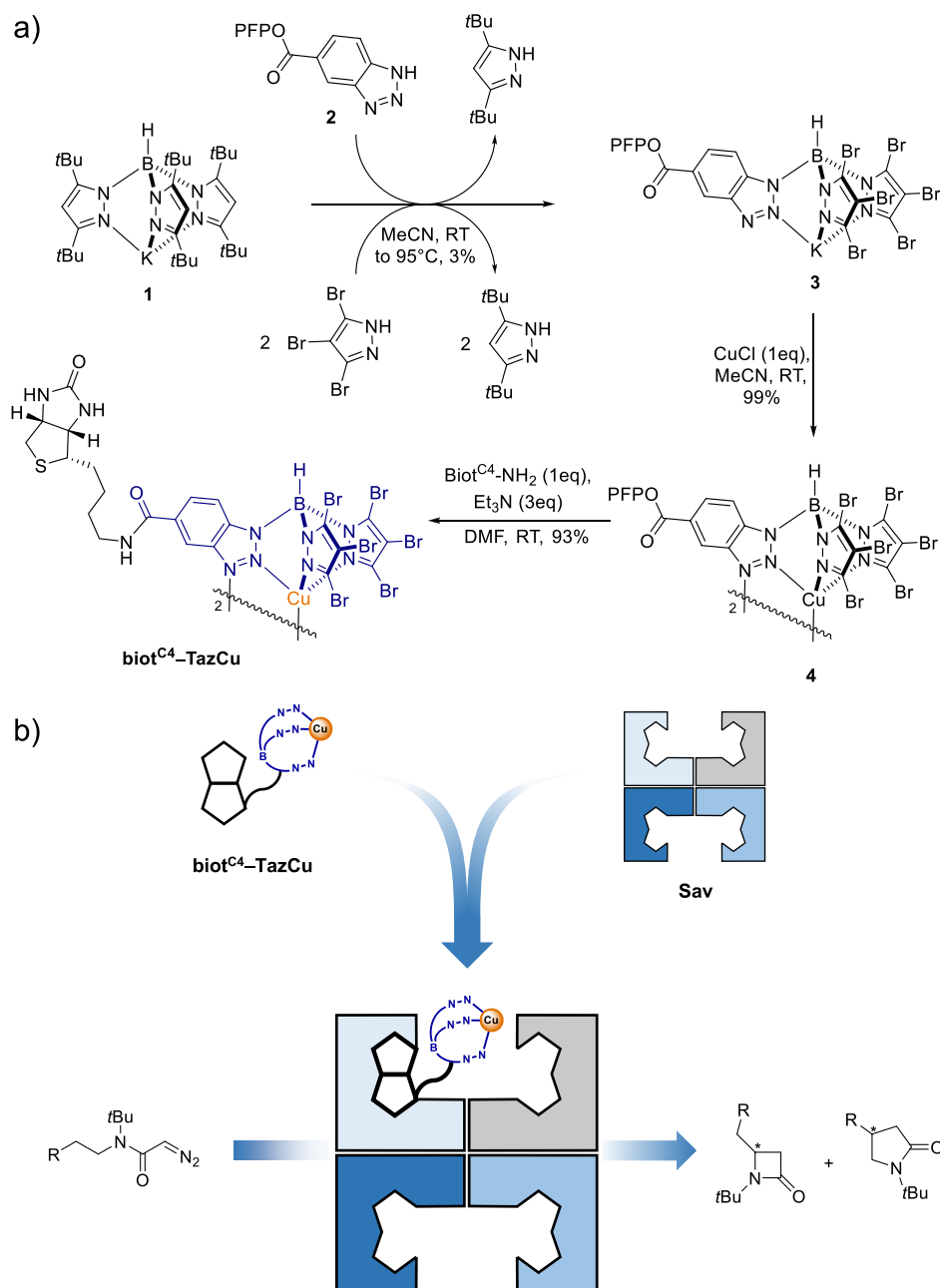
regioisomers when substrates containing different C−H bonds were subjected to functionalization.

With the aim of combining the benefits of homogeneous and enzymatic catalysts, artificial metalloenzymes (ArMs) have attracted increasing attention since the pioneering work of Wilson and Whitesides.[14−17] The anchoring of an abiotic catalytic moiety within a protein enables combining of attractive assets of both homogeneous and enzymatic catalysis.[17−21] Certain natural enzymes including S-adenosyl methionine-dependent (SAM) enzymes catalyze the alkylation of C−H bonds. They are however mainly limited to the transfer of methyl groups or highly specific C−C bonds with radical acceptors.[22,23] Repurposed (natural) enzymes and ArMs offer an attractive means to complement SAM-dependent enzymes for C−H activation purposes.[21,24−28] Among the most noteworthy achievements in "new-to-nature" C−C bond formation via C−H functionalization, one should mention engineered P411,[29,30] repurposed P450,[31−34] my-

Scheme 1. Artificial Metalloenzyme for C–H Insertion Resulting from Anchoring a Biotinylated Copper(I) Heteroscorpionate Complex in Sav (Streptavidin)[a]

[a](a) Synthesis of the cofactor via pyrazole/triazole metathesis on Tp$^{(tBu)2}$K **1** and conjugation with a modified biotin anchor to afford the cofactor **biot^{C4}–TazCu**. PFP = pentafluorophenyl; (b) artificial metalloenzyme assembly via supramolecular anchoring of **biot^{C4}–TazCu** into Sav. The assembled artificial metalloenzyme catalyzes the formation of β- and γ-lactams via intramolecular C–H insertion of carbene intermediates.

oglobin,[35,36] and streptavidin[37,38] ArMs. However, examples of highly active C–H insertion biocatalysts that are based on first-row transition metals and tolerate aerobic reaction conditions remain scarce. The work presented herein capitalizes on a Cu(I) heteroscorpionate complex to engineer a highly active ArM that catalyzes the intramolecular insertion of carbenes into different types of C–H bonds in a regio- and enantioselective fashion.

RESULTS AND DISCUSSION

Cofactor Synthesis and Computational Modeling. The remarkable affinity of biotin for streptavidin ($K_d < 10^{-13}$

M) offers an attractive means to anchor any biotinylated probe within streptavidin (Sav). Several groups have relied on this tool to assemble ArMs.[14,37–46] A common strategy for the synthesis of anchored Tp complexes relies on the introduction of a fourth substituent on the boron, replacing the hydride moiety.[47–49] In our hands, however, this strategy proved challenging as tetrasubstituted Tp-derivatives bearing electron-deficient pyrazoles revealed insufficient stability. Inspired by the work of Desrochers and co-workers on heterocycle metathesis,[50] we selected the Tp$^{(tBu)2}$K **1** as the precursor for the assembly of a biotinylated, electron-deficient TpM-cofactor. The pronounced steric bulk around the boron

enabled the selective substitution of the three *tert*-butyl pyrazole groups by the benzotriazole **2** bearing an activated ester and two tribromopyrazole moieties to afford the intermediate **3**, albeit in low yield, as shown in Scheme 1a. This intermediate was characterized by X-ray crystallography (Figure S1). Trans-metalation with cuprous chloride yielded compound **4**, which was also characterized by X-ray crystallography (Figure S2). Interestingly, the structure revealed that the benzotriazole coordinates to a second copper center through the third nitrogen to afford a dimeric structure. To ensure additional electron-deficient character to the cofactor, the benzotriazole was equipped with a carboxylate moiety. Coupling to biotin thus required the use of biotin–amine (i.e., **biot^{C4}–NH$_2$**),[51] rather than biotin, which bears a valeric acid. The biotinylated cofactor **biot^{C4}–TazCu** was assembled by reacting **biot^{C4}–NH$_2$** with the activated ester **4** to ensure its localization within Sav, as shown in Scheme 1b. High-resolution mass spectrometry (HRMS) and detailed nuclear magnetic resonance (NMR) analysis enabled unambiguous characterization of the biotinylated cofactor **biot^{C4}–TazCu** (see Supporting Information Figures S3–S5).

The quantitative anchoring of the cofactor **biot^{C4}–TazCu** into Sav was assessed via CD spectroscopy, as shown in Figure S6.[52] The overall binding affinity relies on a one-to-one binding stoichiometry with the mathematical expression derived in the Supporting Information (Figure S6).[53] The fitted dissociation constant was $K_d = 2.37 \pm 1.40 \cdot 10^{-8}$ M, thus leading to >99% of bound **biot^{C4}–TazCu** in the presence of equimolar concentrations of the cofactor and tetrameric Sav. Unfortunately, all attempts to crystallize the ArM: **biot^{C4}–TazCu·Sav WT** were vain. Accordingly, we turned to quantum mechanics/molecular mechanics (QM/MM) calculations to model **biot^{C4}–TazCu·Sav WT** ArM (see the Supporting Information for details). Both the HABA displacement titration and the QM/MM modeling confirmed that up to four **biot^{C4}–TazCu** cofactors could be accommodated in the homotetrameric host Sav WT. Amino acids that point toward the docked Cu-center include K121, S112, and L124 with a second, more remote shell that includes T114, T115, and N118, Figure 1. Based on the computed structure, we selected residues K121, S112, and L124 for the genetic optimization of the ArM.

Single-Mutant Screening. Reports by Pérez and co-workers suggest that sterically hindered diazoacetamides are less prone to undergo homocoupling in copper tris(pyrazolyl)-borate-catalyzed intramolecular C–H insertion reactions.[54] The diazoacetamide substrate **5** was selected for initial screening, as shown in Table 1. This reaction is of particular interest as it provides a straightforward access to *β*- and *γ*-lactams upon C–H insertion. These represent ubiquitous structural motifs in numerous pharmaceutically relevant compounds.[55–57] Similarly, Fasan and co-workers reported the stereoselective formation of fused *γ*-lactams via biocatalytic intramolecular cyclopropanation of diazoacetamide.[58]

As the cofactor's activity was affected by the presence of cellular metabolites, we adapted a purification protocol of Sav mutants in a 96-well plate based on our streamlined protocol.[59] Cytoplasmic protein overexpression was carried out in the *E. coli* strain BL21 (DE3) in 24-deep-well plates. Following cell lysis and centrifugation, the cell-free extract was applied to an iminobiotin-Sepharose resin under basic conditions (pH = 10.6, 100 mM carbonate buffer), leading to the immobilization of Sav on the resin. After washing (pH = 7.9, 100 mM MOPS
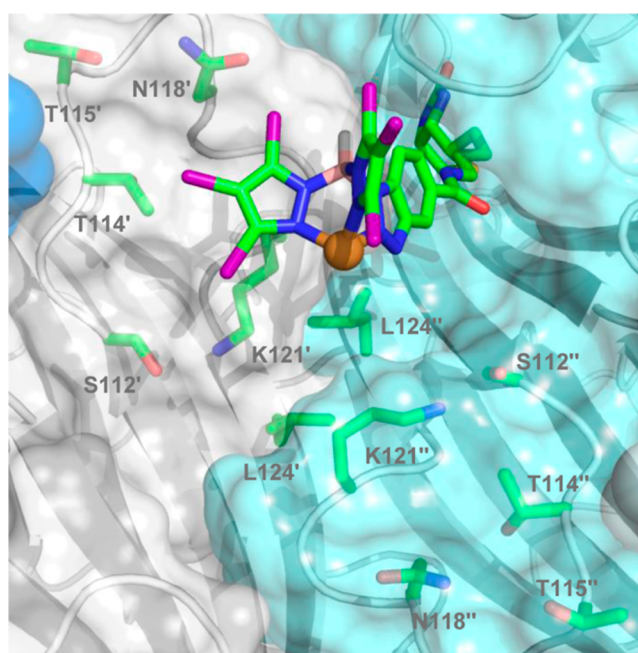

Figure 1. Close-up view of the structure resulting from modeling **biot^{C4}–TazCu** within Sav WT. The cofactor was docked into one monomer (Sav′, gray), leaving the adjacent (Sav″, pale blue) binding site empty. Cu–C$_\beta$ distances (Å) of the closest-lying amino acid: S112′ (11.8); T114′ (11.9); T115′ (14.3); N118′ (10.1); K121′ (8.1); L124′ (13.8); S112″ (10.5); T114″ (12.3); T115″ (15.6); N118″ (12.2); K121″ (9.9); L124″ (12.9). Sav is displayed as a transparent solvent-accessible surface overlaid with a cartoon representation of the 8-stranded *β*-barrel. Close-lying residues and the **biot^{C4}–TazCu** cofactor are displayed as color-coded sticks and Cu as an orange sphere.

buffer), elution with an acidic solution (pH = 5.5, 100 mM MES buffer) led to protonation of the iminobiotin, thus releasing Sav. Its concentration in the elution buffer was determined via a fluorescence assay with biotin-4-fluorescein, as shown in Figure S7. Concentrations >5 μM Sav (tetramer, >20 μM biotin-binding sites) were obtained for most of the Sav mutants. Early catalytic experiments revealed a decrease in performance with decreasing Sav: **biot^{C4}–TazCu** ratios (i.e. 1,:1 vs 1:4). We surmise that binding of two **biot^{C4}–TazCu** in adjacent biotin-binding sites impedes catalytic activity. Accordingly, an excess of biotin-binding sites in the reaction was enforced (e.g., >4 equiv of Sav monomers vs 1 equiv of the cofactor).

To evaluate the effect of residual cellular debris, a culture of *E. coli* harboring an empty plasmid (i.e., no Sav overexpressed) was subjected to the above iminobiotin purification protocol. The collected eluate was evaluated in catalysis at pH 6.5 in the presence of 1 μM of either complex **4** or **biot^{C4}–TazCu** (0.02% loading) and the diazoacetamide substrate **5**, as shown in Table 1, entries 2 and 3. A 1:3 mixture of racemic *β*/*γ* lactams **6a** and **6b** was obtained with a total turnover number (TTON) of 371 and 458, respectively. To our disappointment, upon incorporation in WT Sav, no conversion could be detected by supercritical fluid chromatography (SFC); see Table 1 (entry 20). As both lysine residues K121 and K121′ were computed to lie closest to Cu, we initiated our genetic optimization efforts by mutating this position. Gratifyingly, the ArM **biot^{C4}–TazCu·Sav K121A** proved catalytically active and afforded >900 TTONs with a 1:2 r.r. (*β*/*γ*, i.e., **6a:6b**) but as a

Table 1. Summary of the Screening Results of biot^{C4}−TazCu·Sav K121X for the C−H Insertion in the Presence of Substrate 5

entry	SAV	TON^a	e.r.^{a}	TON^a	e.r.^{a}	r.r. (β/γ)	TTON (yield (%))
1^{b,c}		ND		ND			ND
2^c	empty vector	91	50:50	280	50:50	24:76	371(7,4)
3	empty vector	112	50:50	346	49:51	24:76	458(9,2)
4	K121A	334	49:51	577	48:52	37:63	912(18,2)
5	K121I	741	40:60	1708	49:51	30:70	2449(49,0)
6	K121L	594	36:64	1693	34:66	26:74	2287(45,7)
7	K121M	109	52:48	317	45:55	26:74	426(8,5)
8	K121V	550	41:59	1124	50:50	33:67	1674(33,5)
9	K121F	709	37:63	1449	64:36	33:67	2157(43,1)
10	K121W	588	38:62	870	49:51	40:60	1458(29,2)
11	K121Y	718	39:61	923	46:54	44:56	1640(32,8)
12	K121C	511	44:56	768	50:50	40:60	1280(25,6)
13	K121N	312	43:57	358	45:55	47:53	670(13,4)
14	K121Q	390	40:60	506	48:52	44:56	895(17,9)
15	K121S	549	42:58	645	51:49	46:54	1192(23,8)
16	K121T	329	41:59	650	45:55	34:66	979(19,6)
17	K121D	62	48:52	146	52:48	30:70	208(4,2)
18	K121E	421	40:60	560	52:48	43:57	980(19,6)
19	K121H	ND		ND			ND
20	WT	ND		ND			ND
21	K121R	ND		ND			ND
22	K121G	455	51:49	753	49:51	38:62	1208(24,2)
23	K121P	365	50:50	626	55:45	37:63	991(19,8)

^{a}Determined by chiral SFC using 1,3,5-trimethoxybenzene as the internal standard. ^{b}The reaction was performed in DCM with 5% DMSO and 5% acetone. ^{c}The reaction was performed with complex 4 instead of biot^{C4}−TazCu. ND = not detected.
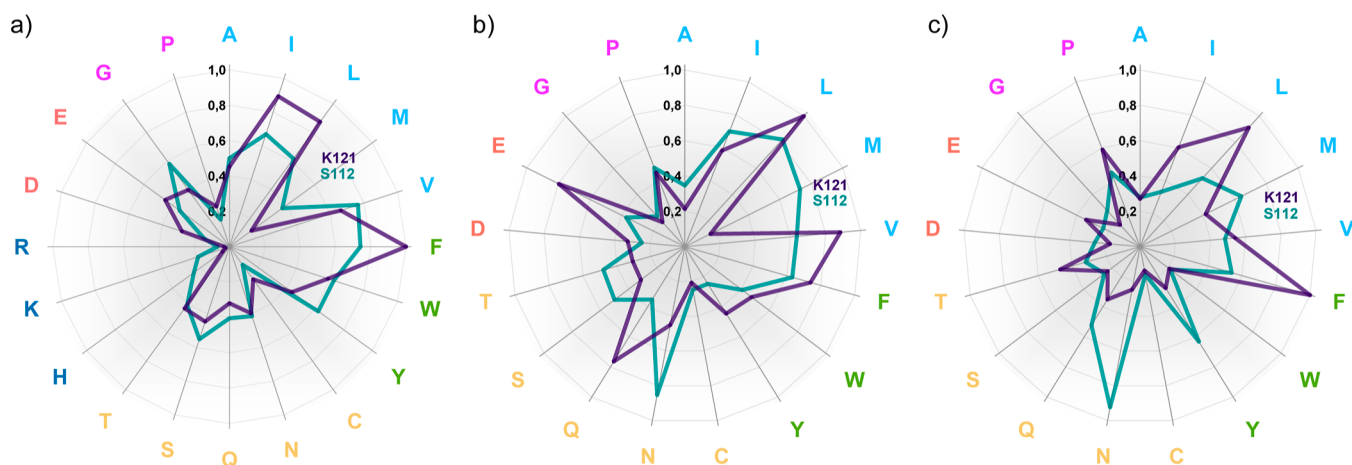

Figure 2. Relative contribution of each amino acid at positions S112 and K121 to (a) TON for C−H insertion (average of all the double mutants for a respective mutation); (b) and (c) enantio-induction for the β-lactam 6a and the γ-lactam 6b, respectively (average of the absolute enantiomeric excess value for all the double mutants with a respective mutation). Amino acids with similar properties are highlighted in the same color (light blue: apolar; green: aromatic; yellow: polar nonionic; dark blue: basic; red: acidic; purple: special). The enantioselectivity obtained with residues H, K, and R is not displayed due to the very low conversions.

(near) racemate; see entry 4. Next, we screened the ArMs resulting from saturation mutagenesis at position Sav K121X; see Table 1. As can be appreciated, the nature of the residue at Sav K121X significantly affects the catalytic performance. From these results, the following trends emerge: positively charged residues at position K121 (Lys, His, and Arg) consistently shut

down activity (entries 19, 20, and 21). We hypothesize that such close-lying, potentially coordinating Lewis basic residues may coordinate with the Cu(I), and prevent the formation of the Cu−carbene moiety. On the other hand, apolar (Ile, Leu, and Val) and aromatic residues (Phe, Trp, and Tyr) have a beneficial effect on activity (entries 5, 6, 8, 9, 10, and 11). The
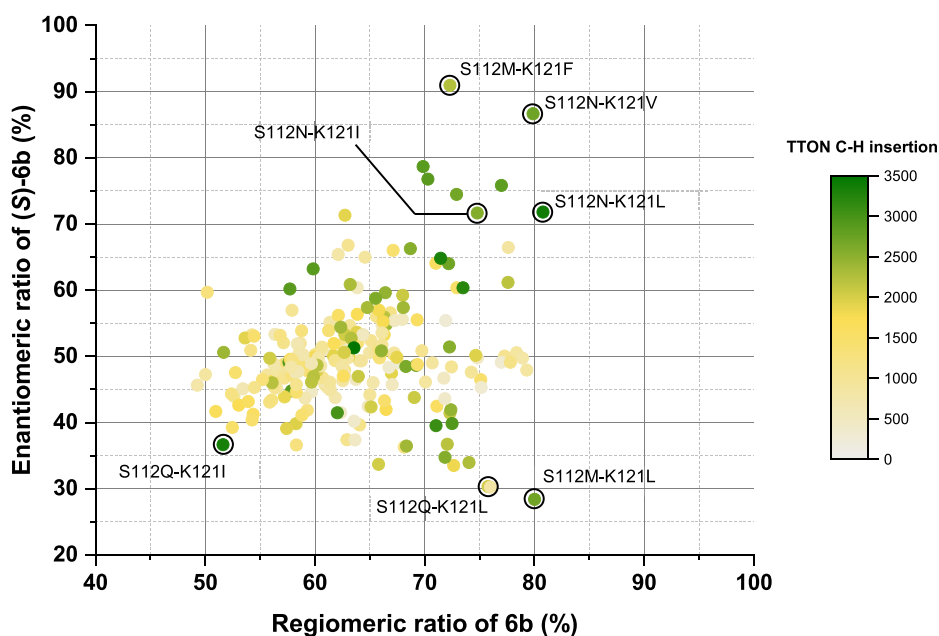
Figure 3. Graphical summary of the screening results of **biot**^{C4}−**TazCu**·Sav S112X K121X′ for the C−H insertion of substrate **5** to afford lactams **6a** and **6b**. The axes display the enantiomeric and the regiomeric ratios of the γ-lactam (S)-**6b**. Key mutations leading to high e.r. and r.r. include asparagine and methionine at position S112 and a hydrophobic residue at K121.

ArM **biot**^{C4}−**TazCu**·Sav K121L provided 74% γ-lactam with the highest enantiomeric ratios (36:64 and 34:66 for **6a** and **6b**, respectively) of the single mutants (entry 6). ArM **biot**^{C4}−**TazCu**·Sav K121I displayed the highest activity with 2648 TTON, corresponding to 53% yield (i.e., assay yield, used throughout unless specified). Polar uncharged residues (Asp, Glu, Asn, Gln, Ser, and Thr) generally yielded lower conversions than their apolar counterparts. Interestingly, the mutant bearing an aspartate (entry 17) impeded the reaction much more than its glutamate homologue (entry 18). Similar effects on the turnover number (TON) and e.r. could also be observed between the two isosteric residues cysteine and serine (entries 12 and 15). Overall, a large hydrophobic residue at Sav K121I/L/F appeared essential to maximize the three figures of merit TTON, r.r., and e.r. Interestingly, the ArM also afforded non-negligible amounts of the Büchner ring-expansion product depending on the mutant tested (see the Supporting Information for details). Water insertion and diazo-coupling byproducts could be detected by ESI−MS of the catalytic reactions but were not investigated further (Scheme S2). Although reported for C−H bonds of methyl groups in Rh- and TpCu-based catalysts,[54,60] C−H insertion into the *tert*-butyl group was not detected, thus minimizing the formation of additional regioisomers.

Double-Saturation Mutagenesis. With the aim of identifying synergistic interactions between residues K121 and S112, we set out to screen the double-saturation mutagenesis library comprising the 400 Sav isoforms Sav S112X K121X′. Of the 400 double mutants, 362 could be screened and 220 afforded detectable levels of activity (see Table S1). The general trends observed in the single-mutant Sav K121X screening were confirmed for the double mutants. Positively charged residues (His, Lys, and Arg) consistently impeded activity, particularly at position K121, where none of

the three were tolerated, irrespective of the nature of residue S112X, as shown in Figure 2a. Proline and cysteine displayed a deleterious influence as well at both S112 and K121 positions. The unexpected difference between the homologous amino acids aspartate and glutamate was also visible in this screening. The aspartate residue proved to be less advantageous than glutamate at both positions. An apolar side chain (aliphatic or aromatic) at position K121 turned out to be an absolute requirement to obtain a higher activity of the ArM. While the two isoforms leucine and isoleucine provided comparable levels of activity at positions K121 and S112, a pronounced difference in enantioselectivity was observed, as shown in Figure 2b,c. The leucine residue afforded much higher levels of enantio-induction for both the β-lactam **6a** and the γ-lactam **6b** on average. The asparagine at position S112 appeared to be crucial for enantioselectivity for both reaction products. Among other occurrences, K121V, K121E, and K121Q had a positive influence on the enantioselective formation of **6a** but turned out to be less relevant for the other regioisomer **6b**.

To help identify a suitable double mutant subject to another round of directed evolution, we analyzed e.r., r.r., and TTON by displaying the e.r. versus r.r. for the γ-lactam (+)-**6b**, as shown in Figure 3. The absolute configuration of the γ-lactam (+)-**6b** was determined as (S)-**6b** by comparison with the secondary amide (deprotected, following treatment of (+)-**6b** with TFA).[61] The data reveal a clear trend for the functionalization of the benzylic position. Both enantiomers of the γ-lactam **6b** could be accessed, albeit with a higher enantioselectivity for the (S)-**6b**. Interestingly, mutation of the K121L to K121F while conserving the S112M residue allowed us to invert the enantioselectivity from 28:72 to 91:9 e.r. Variants S112N−K121L and S112N−K121I revealed similar performance. Strikingly, substitution of S112N for S112Q led to an inversion of enantioselectivity (e.g., S112N K121L/I and

S112Q_K121L/I afford (*S*)-**6b** and (*R*)-**6b**, respectively). Of note, a pronounced difference in regioselectivity was observed between S112Q-K121L and S112Q-K121I, the former clearly favoring the formation of the γ-lactam **6b**, as shown in Figure 3.

High levels of activity, regioselectivity, and enantioselectivity could be obtained with the S112N−K121V variant (86:14 e.r., 80% regioselectivity and 2731 TTON). On average, the valine residue did not display as high levels of enantioselectivity as leucine or phenylalanine for **6b**, as shown in Figure 2c. This finding highlights the importance of cooperative effects between sites and would not have been identified with an iterative single-site-saturation strategy.

The β-lactam **6a** product could not be obtained in >51% r.r. and modest conversion (<10%, < 500 TON). The higher bond dissociation energy of the amide's vicinal C−H bond (BDE ≈ 93 kcal/mol vs 87 kcal/mol for the benzylic C−H bond, predicted with ALFABET from the corresponding acetamide)[62] and the ring strain in the transition state leading the four-membered β-lactam **6a** both favor the formation of the γ-lactam **6b**. In some occurrences, considerable amounts of the Büchner ring-expansion product were detected. This was particularly pronounced when position S112 contained an aromatic residue (i.e., S112Y or S112F: up to 1783 TON for S112F−K121I; see Figure S8 and Table S2). The second coordination sphere of Sav could also induce enantioselectivity for this transformation (up to 24:76 e.r. for S112F−K121I). Detailed data for selected mutants are collected in Table S3.

L124 Saturation Mutagenesis and Substrate Scope. Critical inspection of the results of the double-saturation mutagenesis screening led us to select the double mutant Sav S112N−K121V for the next round of directed evolution, focusing on residue Sav L124. A library encoding all 20 amino acids was prepared, relying on NDT, VMA, ATG, and TGG codons. The screening revealed that the size of the amino acid at position L124 had a significant impact on both the e.r and r.r. The triple mutant Sav S112N−K121V−L124I led to slightly improved e.r. (88:12) and r.r (14:86) for the γ-lactam (*S*)-**6b**, as shown in Figure 4. Strikingly, substitution of the bulky hydrophobic L121I residue by a glycine, Sav S112N−K121V−L124G, led to the preferential formation of the β-lactam **6a** with 65:35 r.r. (compared to 19:81 for the parent double mutant) at the cost of a lower TTON. Interestingly, the enantioselectivity was reversed, favoring the β-lactam (−)-**6a** (identified as the (*R*)-enantiomer by vibrational circular dichroism spectrometry; see the Supporting Information for details). Attempts to further improve the catalytic performance by applying site-saturation mutagenesis at positions T114, T115, and N118 did not lead to any improvement for either TTON, r.r., or e.r.

To further investigate the performance of the earth-abundant ArM, we selected substrates with either a shorter or longer aliphatic chain, as shown in Table 2. Substrate **7** yielded the corresponding β-lactam (+)-**8a** (corresponding to (*R*)-**8a**)[63] in 1290 TON and e.r. of 79:21 with **biot**[C4]−**TazCu**·Sav S112N−K121L. To verify if the selective formation of the γ-lactam **6b** was caused by the lower BDE of the benzylic C−H bond (BDE ≈ 87 kcal/mol, predicted with ALFABET from the corresponding acetamide),[62] we also subjected substrate **9** bearing a propylene spacer (BDE ≈96 kcal/mol for the homobenzylic C−H bond) to the transformation. To our delight, the γ-lactam **10b** was obtained with 3585 TON, 88% regioselectivity, and 27:73 e.r with **biot**[C4]−**TazCu**·Sav
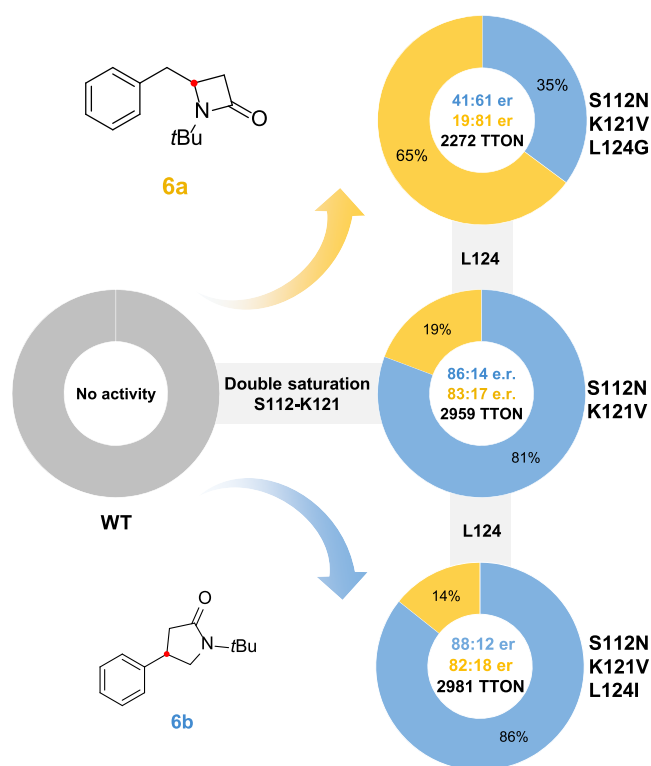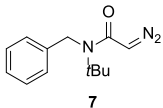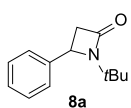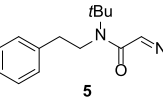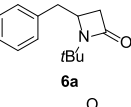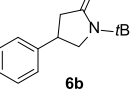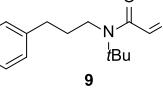

Figure 4. Evolutionary lineage of the ArM for regio- and enantioselective C−H insertion. Initial double-saturation mutagenesis on WT Sav to identify improved double mutants was followed by single-site-saturati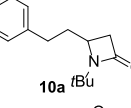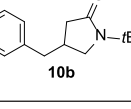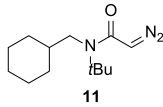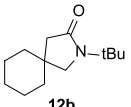on mutagenesis at position L124. Mutation of L124 with an isoleucine slightly increased the selectivity of the ArM for the γ-lactam (*S*)-**6b**, while a glycine residue favors the β-lactam (−)-**6a**. The data are the average of biological triplicates.

S112N−K121V. However, regioselectivity could not be tuned to favor the β-lactam **10a** when **biot**[C4]−**TazCu**·Sav S112N−K121V−L124G was used: only a modest increase from 12 to 28% β-lactam **10a** was observed. The ArM also catalyzed the carbene insertion into a tertiary C−H bond (BDE ≈ 93 kcal/mol)[62] with high efficiency: **biot**[C4]−**TazCu**·Sav S112N−K121L afforded the spirocyclic γ-lactam **12b** in 93% yield and 4627 TON. The four-membered ring regioisomer could not be detected either by ^{1}H NMR or HPLC. A selection of para-substituted derivatives of substrate **5** was also tested. Significantly lower TON and selectivities were observed, independently of the nature of the substituent. This highlights a preference of the ArM for unsubstituted phenyl rings. Detailed data are collected in Table S4.

CONCLUSIONS

While Tp complexes can efficiently functionalize inert sp[3] C−H bonds by insertion of a reactive carbene intermediate, the absence of interactions between the metal and the substrate render the selectivity of the reaction challenging to control. This study reveals that this challenge can be addressed by providing a well-structured second coordination sphere around the transition state. The synthesis of a modified biotin-bearing copper(I) heteroscorpionate enabled its incorporation into a genetically evolvable host protein. The resulting ArM catalyzes the enantio- and regioselective formation of β- and γ-lactams via the insertion of a carbene intermediate into secondary and tertiary sp[3] C−H bonds. Double-saturation mutagenesis and directed evolution at a third position shed light on individual

Table 2. Selected Results for the Intramolecular C−H Insertion Catalyzed by biot^{C4}−TazCu·Sav mutants^a

Substrate	Product	Mutant	e.r. (+/-)	r.r. (β/γ)	TTON (Yield (%))^b
7	8a	S112N-K121L	79:21	-	1290 (25.8)
5	6a	S112N-K121V-L124G	19:81	65:35	2272 (45.4)
	6b	S112N-K121V-L124I	88:12	14:86	2981^c (59.6)
9	10a	S112N-K121V-L124G	37:63	28:72	2623 (52.5)
	10b	S112N-K121V	27:73	12:88	3585 (71.7)
11	12b	S112N-K121L	-	0:100	4627 (92.5)^d

^{a}Conditions: 5 mM substrate, 1 μM biot^{C4}−TazCu, >1 μM Sav$_{tet}$, 35 mM MES pH 5.5, 10% acetone, 5% DMSO, 15 h at 25 °C under air. ^{b}Yields were determined by SFC with 1,3,5-trimethoxybenzene as the internal standard. ^{c}This reaction was also performed on a preparative scale; see Table S1 and Figures S9 and S10. ^{d}Yield determined by ^{1}H NMR with 1,3,5-trimethoxybenzene as the internal standard.

amino acid contributions to the cofactor's activity. TONs up to 4627 (corresponding to 93% yield) in the case of the C−H insertion into a cyclohexyl substituent were achieved. We envision that the use of the highly versatile scorpionate complexes for ArMs could open new opportunities to expand the enzymatic repertoire of C−H functionalization strategies, based on earth-abundant metal cofactors.

ASSOCIATED CONTENT

Supporting Information

The Supporting Information is available free of charge at https://pubs.acs.org/doi/10.1021/jacs.2c03311.

General information, experimental section, schemes, figures, tables, and X-ray reports (PDF)

Accession Codes

CCDC 2151848−2151849 contain the supplementary crystallographic data for this paper. These data can be obtained free of charge via www.ccdc.cam.ac.uk/data_request/cif, or by emailing data_request@ccdc.cam.ac.uk, or by contacting The Cambridge Crystallographic Data Centre, 12 Union Road, Cambridge CB2 1EZ, UK; fax: +44 1223 336033.

AUTHOR INFORMATION

Corresponding Author

Thomas R. Ward − *Department of Chemistry, University of Basel, Basel CH-4058, Switzerland;* orcid.org/0000-0001-8602-5468; Email: thomas.ward@unibas.ch

Authors

Corentin Rumo − *Department of Chemistry, University of Basel, Basel CH-4058, Switzerland;* orcid.org/0000-0001-7411-5212

Alina Stein − *Department of Chemistry, University of Basel, Basel CH-4058, Switzerland;* orcid.org/0000-0002-2526-506X

Juliane Klehr − *Department of Biomedizin, University of Basel, Basel CH-4031, Switzerland*

Ryo Tachibana − *Department of Chemistry, University of Basel, Basel CH-4058, Switzerland*

Alessandro Prescimone − *Department of Chemistry, University of Basel, Basel CH-4058, Switzerland;* orcid.org/0000-0002-3631-5210

Daniel Häussinger − *Department of Chemistry, University of Basel, Basel CH-4058, Switzerland;* orcid.org/0000-0002-4798-0072

Complete contact information is available at:
https://pubs.acs.org/10.1021/jacs.2c03311

Notes

The authors declare no competing financial interest.

ACKNOWLEDGMENTS

■ REFERENCES

(1) Bergman, R. G. C−H Activation. *Nature* **2007**, *446*, 391−393.

(2) Dalton, T.; Faber, T.; Glorius, F. C−H Activation: Toward Sustainability and Applications. *ACS Cent. Sci.* **2021**, *7*, 245−261.

(3) Hartwig, J. F.; Larsen, M. A. Undirected, Homogeneous C−H Bond Functionalization: Challenges and Opportunities. *ACS Cent. Sci.* **2016**, *2*, 281−292.

(4) Sambiagio, C.; Schönbauer, D.; Blieck, R.; Dao-Huy, T.; Pototschnig, G.; Schaaf, P.; Wiesinger, T.; Zia, M. F.; Wencel-Delord, J.; Besset, T.; Maes, B. U. W.; Schnürch, M. A Comprehensive Overview of Directing Groups Applied in Metal-Catalysed C−H Functionalisation Chemistry. *Chem. Soc. Rev.* **2018**, *47*, 6603−6743.

(5) Straub, B. F. Organotransition Metal Chemistry. From Bonding to Catalysis. *Angew. Chem., Int. Ed.* **2010**, *49*, 7622.

(6) Zheng, C.; You, S.-L. Recent Development of Direct Asymmetric Functionalization of Inert C−H Bonds. *RSC Adv.* **2014**, *4*, 6173−6214.

(7) Gillingham, D.; Fei, N. Catalytic X−H Insertion Reactions Based on Carbenoids. *Chem. Soc. Rev.* **2013**, *42*, 4918−4931.

(8) Davies, H. M. L.; Beckwith, R. E. J. Catalytic Enantioselective C−H Activation by Means of Metal−Carbenoid-Induced C−H Insertion. *Chem. Rev.* **2003**, *103*, 2861−2904.

(9) Muñoz-Molina, J. M.; Belderrain, T. R.; Pérez, P. J. Trispyrazolylborate Coinage Metals Complexes: Structural Features and Catalytic Transformations. *Coord. Chem. Rev.* **2019**, *390*, 171−189.

(10) Díaz-Requejo, M. M.; Pérez, P. J. Copper, Silver and Gold-Based Catalysts for Carbene Addition or Insertion Reactions. *J. Organomet. Chem.* **2005**, *690*, 5441−5450.

(11) Díaz-Requejo, M. M.; Pérez, P. J. The TpxM Core in Csp3−H Bond Functionalization Reactions: Comparing Carbene, Nitrene, and Oxo Insertion Processes (Tpx = Scorpionate Ligand; M = Cu, Ag). *Eur. J. Inorg. Chem.* **2020**, *2020*, 879−885.

(12) Caballero, A.; Despagnet-Ayoub, E.; Mar Díaz-Requejo, M.; Díaz-Rodríguez, A.; González-Núñez, M. E.; Mello, R.; Muñoz, B. K.; Ojo, W.-S.; Asensio, G.; Etienne, M.; Pérez, P. J. Silver-Catalyzed C-C Bond Formation Between Methane and Ethyl Diazoacetate in Supercritical CO2. *Science* **2011**, *332*, 835−838.

(13) Gava, R.; Olmos, A.; Noverges, B.; Varea, T.; Álvarez, E.; Belderrain, T. R.; Caballero, A.; Asensio, G.; Pérez, P. J. Discovering Copper for Methane C−H Bond Functionalization. *ACS Catal.* **2015**, *5*, 3726−3730.

(14) Wilson, M. E.; Whitesides, G. M. Conversion of a Protein to a Homogeneous Asymmetric Hydrogenation Catalyst by Site-Specific Modification with a Diphosphinerhodium(I) Moiety. *J. Am. Chem. Soc.* **1978**, *100*, 306−307.

(15) Reetz, M. T. Biocatalysis in Organic Chemistry and Biotechnology: Past, Present, and Future. *J. Am. Chem. Soc.* **2013**, *135*, 12480−12496.

(16) Schwizer, F.; Okamoto, Y.; Heinisch, T.; Gu, Y.; Pellizzoni, M. M.; Lebrun, V.; Reuter, R.; Köhler, V.; Lewis, J. C.; Ward, T. R. Artificial Metalloenzymes: Reaction Scope and Optimization Strategies. *Chem. Rev.* **2018**, *118*, 142−231.

(17) Chen, K.; Arnold, F. H. Engineering New Catalytic Activities in Enzymes. *Nat. Catal.* **2020**, *3*, 203−213.

(18) Hönig, M.; Sondermann, P.; Turner, N. J.; Carreira, E. M. Enantioselective Chemo- and Biocatalysis: Partners in Retrosynthesis. *Angew. Chem., Int. Ed.* **2017**, *56*, 8942−8973.

(19) Jeschek, M.; Panke, S.; Ward, T. R. Artificial Metalloenzymes on the Verge of New-to-Nature Metabolism. *Trends Biotechnol.* **2018**, *36*, 60−72.

(20) de Souza, R. O. M. A.; Miranda, L. S. M.; Bornscheuer, U. T. A Retrosynthesis Approach for Biocatalysis in Organic Synthesis. *Chem.−Eur. J.* **2017**, *23*, 12040−12063.

(21) Perez-Rizquez, C.; Rodriguez-Otero, A.; Palomo, J. M. Combining Enzymes and Organometallic Complexes: Novel Artificial Metalloenzymes and Hybrid Systems for C−H Activation Chemistry. *Org. Biomol. Chem.* **2019**, *17*, 7114−7123.

(22) Bennett, M. R.; Shepherd, S. A.; Cronin, V. A.; Micklefield, J. Recent Advances in Methyltransferase Biocatalysis. *Curr. Opin. Chem. Biol.* **2017**, *37*, 97−106.

(23) Yokoyama, K.; Lilla, E. A. C−C Bond Forming Radical SAM Enzymes Involved in the Construction of Carbon Skeletons of Cofactors and Natural Products. *Nat. Prod. Rep.* **2018**, *35*, 660−694.

(24) Lewis, J. C.; Coelho, P. S.; Arnold, F. H. Enzymatic Functionalization of Carbon−Hydrogen Bonds. *Chem. Soc. Rev.* **2011**, *40*, 2003−2021.

(25) Upp, D. M.; Lewis, J. C. Selective C−H Bond Functionalization Using Repurposed or Artificial Metalloenzymes. *Curr. Opin. Chem. Biol.* **2017**, *37*, 48−55.

(26) Zhang, R. K.; Huang, X.; Arnold, F. H. Selective CH Bond Functionalization with Engineered Heme Proteins: New Tools to Generate Complexity. *Curr. Opin. Chem. Biol.* **2019**, *49*, 67−75.

(27) Zetzsche, L. E.; Narayan, A. R. H. Broadening the Scope of Biocatalytic C−C Bond Formation. *Nat. Rev. Chem.* **2020**, *4*, 334−346.

(28) Ren, X.; Fasan, R. Engineered and Artificial Metalloenzymes for Selective C−H Functionalization. *Curr. Opin. Green Sustainable Chem.* **2021**, *31*, 100494.

(29) Zhang, R. K.; Chen, K.; Huang, X.; Wohlschlager, L.; Renata, H.; Arnold, F. H. Enzymatic Assembly of Carbon−Carbon Bonds via Iron-Catalysed Sp3 C−H Functionalization. *Nature* **2019**, *565*, 67−72.

(30) Zhang, J.; Huang, X.; Zhang, R. K.; Arnold, F. H. Enantiodivergent α-Amino C−H Fluoroalkylation Catalyzed by Engineered Cytochrome P450s. *J. Am. Chem. Soc.* **2019**, *141*, 9798−9802.

(31) Dydio, P.; Key, H. M.; Nazarenko, A.; Rha, J. Y.-E.; Seyedkazemi, V.; Clark, D. S.; Hartwig, J. F. An Artificial Metalloenzyme with the Kinetics of Native Enzymes. *Science* **2016**, *354*, 102−106.

(32) Key, H. M.; Dydio, P.; Clark, D. S.; Hartwig, J. F. Abiological Catalysis by Artificial Haem Proteins Containing Noble Metals in Place of Iron. *Nature* **2016**, *534*, 534−537.

(33) Gu, Y.; Natoli, S. N.; Liu, Z.; Clark, D. S.; Hartwig, J. F. Site-Selective Functionalization of (Sp^3)C−H Bonds Catalyzed by Artificial Metalloenzymes Containing an Iridium-Porphyrin Cofactor. *Angew. Chem., Int. Ed.* **2019**, *58*, 13954−13960.

(34) Liu, Z.; Huang, J.; Gu, Y.; Clark, D. S.; Mukhopadhyay, A.; Keasling, J. D.; Hartwig, J. F. Assembly and Evolution of Artificial Metalloenzymes within E. Coli Nissle 1917 for Enantioselective and Site-Selective Functionalization of C−H and C=C Bonds. *J. Am. Chem. Soc.* **2022**, *144*, 883−890.

(35) Sreenilayam, G.; Moore, E. J.; Steck, V.; Fasan, R. Metal Substitution Modulates the Reactivity and Extends the Reaction Scope of Myoglobin Carbene Transfer Catalysts. *Adv. Synth. Catal.* **2017**, *359*, 2076−2089.

(36) Vargas, D. A.; Tinoco, A.; Tyagi, V.; Fasan, R. Myoglobin-Catalyzed C−H Functionalization of Unprotected Indoles. *Angew. Chem., Int. Ed.* **2018**, *57*, 9911−9915.

(37) Hyster, T. K.; Knörr, L.; Ward, T. R.; Rovis, T. Biotinylated Rh(III) Complexes in Engineered Streptavidin for Accelerated Asymmetric C−H Activation. *Science* **2012**, *338*, 500−503.

(38) Hassan, I. S.; Ta, A. N.; Danneman, M. W.; Semakul, N.; Burns, M.; Basch, C. H.; Dippon, V. N.; McNaughton, B. R.; Rovis, T. Asymmetric δ-Lactam Synthesis with a Monomeric Streptavidin Artificial Metalloenzyme. *J. Am. Chem. Soc.* **2019**, *141*, 4815−4819.

(39) Facchetti, G.; Rimoldi, I. 8-Amino-5,6,7,8-Tetrahydroquinoline in Iridium(III) Biotinylated Cp* Complex as Artificial Imine Reductase. *New J. Chem.* **2018**, *42*, 18773−18776.

(40) Reetz, M. T. Directed Evolution of Artificial Metalloenzymes: A Universal Means to Tune the Selectivity of Transition Metal Catalysts? *Acc. Chem. Res.* **2019**, *52*, 336–344.

(41) Lewis, J. C. Beyond the Second Coordination Sphere: Engineering Dirhodium Artificial Metalloenzymes To Enable Protein Control of Transition Metal Catalysis. *Acc. Chem. Res.* **2019**, *52*, 576–584.

(42) Lin, C.-C.; Lin, C.-W.; Chan, A. S. C. Catalytic Hydrogenation of Itaconic Acid in a Biotinylated Pyrphos—Rhodium(I) System in a Protein Cavity. *Tetrahedron: Asymmetry* **1999**, *10*, 1887–1893.

(43) Liang, A. D.; Serrano-Plana, J.; Peterson, R. L.; Ward, T. R. Artificial Metalloenzymes Based on the Biotin—Streptavidin Technology: Enzymatic Cascades and Directed Evolution. *Acc. Chem. Res.* **2019**, *52*, 585–595.

(44) Roy, A.; Vaughn, M. D.; Tomlin, J.; Booher, G. J.; Kodis, G.; Simmons, C. R.; Allen, J. P.; Ghirlanda, G. Enhanced Photocatalytic Hydrogen Production by Hybrid Streptavidin-Diiron Catalysts. *Chem.—Eur. J.* **2020**, *26*, 6240–6246.

(45) Santi, N.; Morrill, L. C.; Luk, L. Y. P. Streptavidin-Hosted Organocatalytic Aldol Addition. *Molecules* **2020**, *25*, 2457.

(46) Vornholt, T.; Christoffel, F.; Pellizzoni, M. M.; Panke, S.; Ward, T. R.; Jeschek, M. Systematic Engineering of Artificial Metalloenzymes for New-to-Nature Reactions. *Sci. Adv.* **2021**, *7*, No. eabe4208.

(47) Qin, Y.; Cui, C.; Jäkle, F. Tris(1-Pyrazolyl)Borate (Scorpionate) Functionalized Polymers as Scaffolds for Metallopolymers. *Macromolecules* **2008**, *41*, 2972–2974.

(48) Zagermann, J.; Kuchta, M. C.; Merz, K.; Metzler-Nolte, N. Para-Bromophenyl[Tris(Pyrazolyl)]Borate Complexes of Group 1 Metals, Thallium and Magnesium: Synthesis and Characterization of Transfer Agents for "Third-Generation" Tp Ligands. *Eur. J. Inorg. Chem.* **2009**, *2009*, 5407–5412.

(49) Nakamizu, A.; Kasai, T.; Nakazawa, J.; Hikichi, S. Immobilization of a Boron Center-Functionalized Scorpionate Ligand on Mesoporous Silica Supports for Heterogeneous Tp-Based Catalysts. *ACS Omega* **2017**, *2*, 1025–1030.

(50) Desrochers, P. J.; Besel, B. M.; Corken, A. L.; Evanov, J. R.; Hamilton, A. L.; Nutt, D. L.; Tarkka, R. M. Immobilized Boron-Centered Heteroscorpionates: Heterocycle Metathesis and Coordination Chemistry. *Inorg. Chem.* **2011**, *50*, 1931–1941.

(51) Soares da Costa, T. P.; Tieu, W.; Yap, M. Y.; Zvarec, O.; Bell, J. M.; Turnidge, J. D.; Wallace, J. C.; Booker, G. W.; Wilce, M. C. J.; Abell, A. D.; Polyak, S. W. Biotin Analogues with Antibacterial Activity Are Potent Inhibitors of Biotin Protein Ligase. *ACS Med. Chem. Lett.* **2012**, *3*, 509–514.

(52) Skander, M.; Humbert, N.; Collot, J.; Gradinaru, J.; Klein, G.; Loosli, A.; Sauser, J.; Zocchi, A.; Gilardoni, F.; Ward, T. R. Artificial Metalloenzymes: (Strept)Avidin as Host for Enantioselective Hydrogenation by Achiral Biotinylated Rhodium—Diphosphine Complexes. *J. Am. Chem. Soc.* **2004**, *126*, 14411–14418.

(53) Wang, Z.-X. An Exact Mathematical Expression for Describing Competitive Binding of Two Different Ligands to a Protein Molecule. *FEBS Lett.* **1995**, *360*, 111–114.

(54) Martín, C.; Belderraín, T. R.; Pérez, P. J. Rediscovering Copper-Based Catalysts for Intramolecular Carbon—Hydrogen Bond Functionalization by Carbene Insertion. *ACS Catal.* **2009**, *7*, 4777.

(55) Caruano, J.; Muccioli, G. G.; Robiette, R. Biologically Active γ-Lactams: Synthesis and Natural Sources. *Org. Biomol. Chem.* **2016**, *14*, 10134–10156.

(56) Singh, G. S. Beta-Lactams in the New Millennium. Part-I: Monobactams and Carbapenems. *Mini-Rev. Med. Chem.* **2004**, *4*, 69–92.

(57) Singh, G. S. Beta-Lactams in the New Millennium. Part-II: Cephems, Oxacephems, Penams and Sulbactam. *Mini-Rev. Med. Chem.* **2004**, *4*, 93–109.

(58) Ren, X.; Chandgude, A. L.; Fasan, R. Highly Stereoselective Synthesis of Fused Cyclopropane-γ-Lactams via Biocatalytic Iron-Catalyzed Intramolecular Cyclopropanation. *ACS Catal.* **2020**, *10*, 2308–2313.

(59) Mallin, H.; Hestericová, M.; Reuter, R.; Ward, T. R. Library Design and Screening Protocol for Artificial Metalloenzymes Based on the Biotin-Streptavidin Technology. *Nat. Protoc.* **2016**, *11*, 835–852.

(60) Li, H.; Ma, X.; Lei, M. Substituent Effects and Chemoselectivity of the Intramolecular Buchner Reaction of Diazoacetamide Derivatives Catalyzed by the Di-Rh(II)-Complex. *Dalton Trans.* **2016**, *45*, 8506–8512.

(61) Wee, A. G. H.; Duncan, S. C.; Fan, G. Intramolecular Asymmetric C—H Insertion of N-Arylalkyl, N-Bis(Trimethylsilyl)-Methyldiazoamides Mediated by Chiral Rhodium(II) Catalysts. Synthesis of (R)-β-Benzyl-γ-Aminobutyric Acid. *Tetrahedron: Asymmetry* **2006**, *17*, 297–307.

(62) St. John, P. C.; Kim, Y.; Kim, S.; Paton, R. S.; Paton, R. S. Prediction of Organic Homolytic Bond Dissociation Enthalpies at near Chemical Accuracy with Sub-Second Computational Cost. *Nat. Commun.* **2020**, *11*, 2328.

(63) Pedroni, J.; Boghi, M.; Saget, T.; Cramer, N. Access to β-Lactams by Enantioselective Palladium(0)-Catalyzed C(Sp3)-H Alkylation. *Angew. Chem., Int. Ed.* **2014**, *53*, 9064–9067.